

## ORIGINAL ARTICLE

# Significance of phosphorus inclusions and discrete micron-sized grains of apatite in postglacial forest soils

Gbotemi A. Adediran<sup>1,2</sup>  | Melanie Kielman-Schmitt<sup>3</sup>  | Ellen Kooijman<sup>3</sup>  | Jon-Petter Gustafsson<sup>1</sup> 

<sup>1</sup>Department of Soil and Environment, Swedish University of Agricultural Sciences, Uppsala, Sweden

<sup>2</sup>UK Centre for Ecology and Hydrology, Wallingford, United Kingdom

<sup>3</sup>Department of Geosciences, Swedish Museum of Natural History, Stockholm, Sweden

**Correspondence**

Jon-Petter Gustafsson, Swedish University of Agricultural Sciences, Department of Soil and Environment, SE-750 07 Uppsala, Sweden.

Email: [jon-petter.gustafsson@slu.se](mailto:jon-petter.gustafsson@slu.se)

Gbotemi A. Adediran, UK Centre for Ecology and Hydrology, Wallingford, United Kingdom.

Email: [GboAde@ceh.ac.uk](mailto:GboAde@ceh.ac.uk)

**Funding information**

Svenska Forskningsrådet Formas, Grant/Award Number: 2017-01139; Sveriges Geologiska Undersökning, Grant/Award Number: 36-2044-2016; Vetenskapsrådet, Grant/Award Number: 2021-00276

**Abstract**

Recent advances in soil phosphorus (P) studies have revealed unique P hot spots and discrete micron-sized grains at soil microsites, but the significance of these so-called ‘hot spots’ and grains in P cycling and long-term supply is yet to be determined. We examined soil particles and pore space distribution at a micro-scale in two postglacial forest soils by laser ablation ICP-MS imaging. This allowed us to semi-quantitatively reveal both axial and lateral abundance, distribution, and co-localization of P with elements known to influence its chemical speciation (e.g., Si, Al, Mn, Ca, and Fe). The results show topsoil P to be co-localised predominantly with Si, Al, and Fe. However, in the subsoils, P was co-localised mainly with Ca, Si, Al, and Mg in spots within Si and Al-bearing minerals and with only Ca in discrete micron-sized grains. While the spots of P-Ca inclusions were ~ 1000 µm apart and present at 40–100 cm depth in Tärnsjö, the discrete grains of P-Ca were ~ 700–1200 µm apart and present at 90–100 cm depth in Tönnersjöheden. The P concentrations in these ‘hot spots’ and grains were 7 to 600 times greater than the average soil P concentrations, with the highest values (3434–8716 mmol P kg<sup>-1</sup>) occurring in the C horizons of the two soils. When combined with previous P speciation results obtained by synchrotron P K-edge XANES in the same soils, our work confirms geogenic apatite to have been dissolved in the topsoil and its P transformed to P adsorbed by Al-Si and Fe phases, and to organic P. Most importantly, our work shows subsoil spots of P-Ca inclusions and micron-sized grains to be a long-term source of P and Ca.

**Highlights**

- The significance of high-P spots and discrete grains to long-term P supply is largely unknown.
- For the first time, P concentration and speciation was resolved by LA-ICP-MS multi-elemental analysis.

This is an open access article under the terms of the [Creative Commons Attribution](https://creativecommons.org/licenses/by/4.0/) License, which permits use, distribution and reproduction in any medium, provided the original work is properly cited.

© 2022 The Authors. *European Journal of Soil Science* published by John Wiley & Sons Ltd on behalf of British Society of Soil Science.

- The P spots exist as dispersed apatite inclusions and micron-sized grains in the subsoil.
- P in these spots and grains were up to 600 times greater than the bulk soil P concentrations.

**KEYWORDS**

apatite inclusions, chemical speciation, discrete particles, elemental co-localizations, LA-ICP-MS imaging, phosphorus cycling

## 1 | INTRODUCTION

Phosphorus (P) is one of the most important macronutrients that drive the functioning and productivity rates of the ecosystems and, consequently, the uptake of atmospheric CO<sub>2</sub> by photosynthetic processes (Darcy et al., 2018; Westheimer, 1987). Unlike nitrogen (N), which can be fixed by microorganisms from the large atmospheric N pool, P is mainly released from the lithosphere to the biosphere through the weathering of P-bearing minerals (Filippelli, 2008; Heindel et al., 2018). Over 250 P minerals have been found in nature but, of these, apatite (Ca<sub>5</sub>(PO<sub>4</sub>)<sub>3</sub>(F,Cl,OH)) is the most common and it is found in most igneous, metamorphic, and sedimentary rocks (Fisher, 1973; Heindel et al., 2018; Larsen, 1967). Although other P-bearing minerals such as vivianite and wavellite could be present in some soils (Stelly & Pierre, 1943), the P status of unfertilized soils is commonly linked to P released by weathering of apatite (Filippelli, 2008; Walker & Syers, 1976). The abundance of apatite in soils is therefore one key factor that governs long-term trajectories of P supply in terrestrial ecosystems.

Temperate and boreal forest ecosystems in northern Europe are associated with soils that were formed after the last glaciation 8000–15,000 years ago. Most of these were developed in glacial till and glaciofluvial or wave-washed sand. These forest ecosystems rely on the availability of geogenic P from the soil. Although the limiting nutrient of these ecosystems is typically N rather than P (Högberg et al., 2017), P may be more crucial in the future due to anthropogenic drivers. While natural processes such as soil acidification, apatite dissolution, and leaching lead to slight P losses from these soils, N deposition, as well as whole-tree and stem harvesting, may accelerate P losses over time. For example, a mass balance study carried out for 14,550 Swedish sites revealed that the annual losses of P from forestry exceed 1 kg P ha<sup>-1</sup> in the southern part of Sweden (Akselsson et al., 2008). The potential of postglacial soils to supply the P needed to sustain the growth of temperate and boreal forests over a long period is therefore of significant ecological and economical concern.

Apatite is a relatively soft mineral and is classified among the most easily weathered minerals (Heindel et al., 2018; Larsen, 1967). Although it is relatively insoluble at near-neutral pH, its solubility and weathering rate increase rapidly with increasing acidity, and its concentration in soils is therefore often lower compared to the underlying parent material (Eriksson et al., 2016; Nezat et al., 2008). The depletion of apatite during pedogenesis has been widely documented in several chronosequence studies (Crews et al., 1995; Walker & Syers, 1976; Zhou et al., 2013). It is perceived that apatite is generally more depleted in the top (0–30 cm) soils than the subsoils, and more abundant in young soils (< 20,000 years) than in older soils (Porder & Hilley, 2011; Priezel et al., 2013; Schlesinger et al., 1998; Walker & Syers, 1976). However, substantial depletion of primary apatite has been observed in the surface horizons also of some relatively young soils, especially the ones formed in felsic parent materials and under acidic soil conditions (Adediran et al., 2020; Beck & Elsenbeer, 1999; Blum et al., 2002; Tuyishime et al., 2022). Moreover, depending on the nature of the primary apatite mineral, soil conditions, and weathering intensities, apatite in soils could exist as discrete mineral grains or be preserved as inclusions (i.e., a mineral within another mineral) in a wide range of minerals such as quartz, plagioclase feldspars, biotite, muscovite, and chlorite (Heindel et al., 2018; Nezat et al., 2008; Syers et al., 1967).

Despite the significance of primary apatite in soil P cycling and long-term supply, the quantification of the abundance and distribution of apatite in soil grains and mineral inclusions is difficult. For example, the use of total Ca and P in a bulk soil digest is insufficient to estimate apatite concentrations in soil because both Ca and P are not exclusively found in apatite minerals (Nezat et al., 2007). Moreover, apatite inclusions within unfractured and weathering-resistant silicate minerals are not always exposed to soil solutions and may not dissolve into chemical extractants routinely used in soil P analysis (Nezat et al., 2007; Syers et al., 1967). Nevertheless, several extractants and sequential chemical extraction methods have been developed to estimate apatite in bulk

soils (Blum et al., 2002; Nezat et al., 2007; Syers et al., 1967; Williams et al., 1980). To improve the knowledge of apatite weathering in soils, Heindel et al. recently used scanning electron microscopy (SEM) to develop three matrices: aspect ratio, percent crystal faces, and chemical etching, to estimate the degree of weathering in an isolated apatite grain (Heindel et al., 2018). Out of these matrices, only the aspect ratio (defined as the length of the long axis of an apatite grain divided by the length of the short axis) was significantly correlated with soil extraction indices for apatite dissolution, with rounded apatite grains (low aspect ratios) tending to have higher levels of HCl-extractable P (Heindel et al., 2018). While this method provided valuable information about the morphological characterisation of apatite grains, it is inefficient in characterising the concentrations and molecular speciation of apatite that exist as inclusions in soil.

Apart from the importance of apatite as the primary source of P in soils, the mobility and bioavailability of P in soils are governed by its chemical speciation. For example, once the P in apatite is released upon weathering, it is potentially bioavailable but could also be complexed into other forms by iron (Fe) and aluminium (Al) (hydr)oxides including allophane/imogolite, which are ubiquitous weathering products (Gustafsson et al., 1999; Parfitt, 1989). In addition, P can also be biologically transformed and stored in soil organic matter (Vincent et al., 2012). Hence, P can exist in a variety of chemical forms in soils. Accurate knowledge of the exact P species distribution is required to understand the processes that make P available for plants and to determine the extent of soil P mobilisation and supply over time.

The use of synchrotron-based X-ray fluorescence ( $\mu$ -XRF) microscopy in combination with micro-focused P *K*-edge X-ray absorption near edge structure (XANES) spectroscopy is gaining attention and allows for spatially resolved P chemical speciation in soils at the microscale (Hesterberg et al., 2017; Werner, Mueller, et al., 2017; Yamaguchi et al., 2021). Synchrotron P *K*-edge microspectroscopy was recently used to reveal P hot spots and dust-derived apatite grains in acidic, highly weathered Hawaiian soils (Vogel et al., 2021). We also recently combined P  $\mu$ -XRF imaging with P *K*-edge XANES to study P geochemistry in two postglacial forest soils in Sweden (Adediran et al., 2020). This revealed spatial heterogeneity in P species distribution with most of the P being complexed by Al, Fe, and as organic P in the topsoil. It also revealed hot spots of Ca-bound P consisting of apatite inclusions and discrete micron-sized grains in sub-soils (Adediran et al., 2020). While the combination of  $\mu$ -XRF and P *K*-edge XANES has been useful in resolving P speciation in soil microsites, the approach is insufficient in

resolving the concentrations of P in these so-called 'hot spots' and grains. The significance of the P in these spots and grains and their potential contributions to long-term P supply in soils remains largely unknown.

Laser ablation inductively coupled plasma mass spectrometry (LA-ICP-MS) imaging is a relatively new elemental characterisation and visualisation tool in soil analysis (Arroyo et al., 2009; Arroyo et al., 2010). It is increasingly gaining attention as a sensitive analytical technique with imaging capabilities to characterise the compositions, concentrations, and distributions of multiple elements in soil microsites (Santner et al., 2015; Zaeem et al., 2021). In principle, an LA-ICP-MS system consists of a laser that is used to ablate a sample, which is analysed for elemental composition by an inductively coupled plasma mass spectrometer. The system can be used to generate elemental images by proper synchronisation of the laser ablation unit and the ICP-MS to record transient element intensities at discrete positions on the sample (Santner et al., 2015; Zaeem et al., 2021). Despite the analytical sensitivity, affordability, and high availability of LA-ICP-MS for soil analysis (compared to synchrotron X-ray absorption spectroscopy), the extent to which (semi)quantitative and multi-elemental LA-ICP-MS imaging could be used to deduce soil P abundance, distribution, and speciation, either as a standalone analytical system or in combination with synchrotron XAS, is yet to be investigated.

The objectives of this study are to:

1. Investigate the use of LA-ICP-MS to quantify the concentrations of P at high-P spots and micron-sized grains, and compare the results with average P concentrations in the bulk soils, across soil depths.
2. Utilise spatial multi-elemental imaging and co-localization to resolve the chemical speciation of P and compare the results with direct P speciation analysis by synchrotron P *K*-edge XANES spectroscopy in the same soils.
3. Combine information from the use of quantitative LA-ICP-MS imaging with synchrotron P *K*-edge X-ray fluorescence microscopy and spectroscopy to expand the knowledge of P geochemistry in forest soils.

## 2 | MATERIALS AND METHODS

### 2.1 | Soil sampling and sample preparation

Soil samples from two soil profiles were collected from coniferous forests at Tärnsjö and Tönnersjöheden (coordinates: 60.14° N 16.92° E and 56.42° N 13.40° E

respectively) in Sweden. These soils are relatively young (<12,000 years old) and were formed under a temperate climate. The predominant trees at these sites are *Pinus sylvestris* L. and *Picea abies* Karst (Gustafsson et al., 2015; Zetterberg et al., 2013). The soil at Tärnsjö is an Albic Podzol that was formed in wave-washed sand, whereas the soil at Tönnersjöheden is a podzolized Dystric Arenosol developed in sandy glaciofluvial material (IUSS Working Group WRB, 2014). The P speciation in these soils was recently characterised by both bulk XANES spectroscopy and synchrotron X-ray micro-spectroscopy making them ideal for further studies to achieve the objectives highlighted above (Adediran et al., 2020; Tuyishime et al., 2022). The general soil chemistry of these soils including pseudo-total ( $\text{HNO}_3$ -extractable) P, ammonium oxalate-extractable P, Al, Si, Fe, and Ca, percentage organic carbon (C), and total nitrogen (N) has also been recently characterised (Adediran et al., 2020; Tuyishime et al., 2022).

At Tärnsjö, an eluvial (E) horizon of about 2 cm thick was present beneath the organic horizon. This E horizon was not used in this study since it was highly depleted of P (Adediran et al., 2020). For the current study, B horizon (2–10 and 10–20 cm) and C horizon (40–50 and 90–100 cm) samples were used. The Tönnersjöheden pedon did not have an E horizon, only an A horizon with a gradual transition to the underlying B horizon. The soil samples were gently sieved (<5 mm) to remove stones and debris before air-drying for 72 h. Representative samples from each depth were then embedded in high-purity epoxy resin. Micro-polished petrographic thin sections of 30  $\mu\text{m}$  thick were prepared at TS Lab & Geoservices snc, Cascina, Italy. This sample preparation approach is identical to the one used to prepare the same soils for synchrotron X-ray microspectroscopy in our previous study (Adediran et al., 2020).

## 2.2 | LA-ICP-MS instrumentation and calibration for (semi)quantitative measurement

LA-ICP-MS analysis was performed at the Vegacenter at the Swedish Museum of Natural History using an ESI NWR193 ArF eximer based laser ablation system (Elemental Scientific Lasers, Bozeman, MT, USA) coupled to an Attom high-resolution ICP-MS (Nu Instruments Ltd, Wrexham, UK). The shortest possible transfer line between the two instruments was used to achieve a fast washout time and facilitate optimised spatial resolution and fast analysis. Pre-ablation of the entire soil area was done at a frequency of 2 Hz with a laser spot size of 100  $\mu\text{m} \times 100 \mu\text{m}$  and a translation rate of 150  $\mu\text{m} \text{ s}^{-1}$ . Micron-scale resolution maps (1600  $\mu\text{m} \times 1600 \mu\text{m}$ ) of Na, Mg, Al, Si, P, K, Ca, Mn, and Fe were then acquired at an ablation frequency of 20 Hz with a spot-size of

15  $\mu\text{m} \times 15 \mu\text{m}$ , fluence of 3.5  $\text{J cm}^{-2}$  and a scanning speed of 30  $\mu\text{m} \text{ s}^{-1}$ . The optimised parameters for the LA-ICP-MS measurements are presented in Table S1.

To evaluate the suitability of LA-ICP-MS for quantitative imaging of multiple elements at soil microsites, a primary multi-elemental calibration was performed using the National Institute of Standards and Technology (NIST) standard reference material 610. The quantifications were validated using ERM-CC141 loam soil certified reference material. The certified soil material was embedded in high-purity epoxy resin and a micro-polished petrographic thin section of 30  $\mu\text{m}$  thick was prepared the same way as the experimental soil samples. To account for possible instrument drift during analysis, the certified reference soil material was measured after each of the experimental soil samples.

## 2.3 | LA-ICP-MS data analysis

Qualitative (counts per second) and semi-quantitative (ppm) concentrations of the elements were processed using Iolite 4 software for processing inorganic mass spectrometer data (Paton et al., 2011). Visualisation of multi-elemental abundance and distribution was done using XMapTools, a MATLAB©-based program for electron microprobe X-ray image processing and geothermobarometry (Lanari et al., 2014). This links visualisation with multi-elemental concentration. For example, using the mouse to click on a spot within a map reveals the concentrations of all detected elements at that spot. For every sample analysed, the XMapTools software reports the highest elemental concentrations as well as the average elemental concentrations across the area mapped. This average elemental concentration by LA-ICP-MS is referred to as spatially resolved average concentrations. Two dimensional (2D) images of spatial co-localization of multiple elements in the soils were done using ImageJ (Collins, 2007).

## 3 | RESULTS

### 3.1 | LA-ICP-MS analysis of reference material

The result of multi-elemental quantification by LA-ICP-MS imaging compared to the concentrations of the elements in the certified reference soil materials is presented in Figure 1.

The concentrations of Na, K, and Si were underestimated by LA-ICP-MS imaging (Figure 1). However, the concentrations of P and the major elements that are known to influence its speciation (Ca, Fe, and Al) agreed well with the certified values, with a relative standard

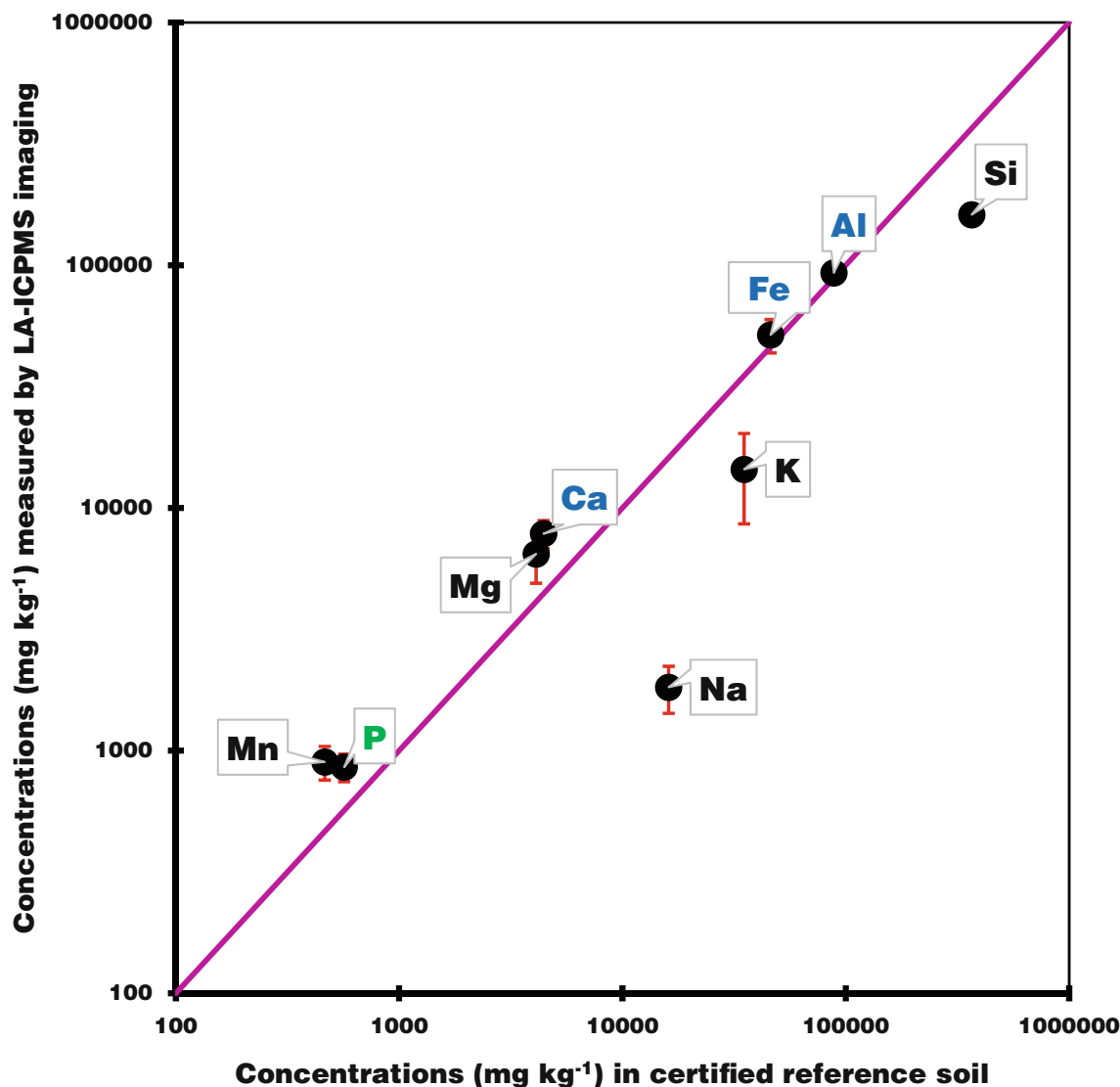


**FIGURE 1** Relationships between concentrations of elements measured by LA-ICP-MS imaging and concentrations of elements in certified reference soil material. The certified soil material was measured after each experimental sample. Data points for each element are average concentrations ( $n = 10$ ) of repeated measurements and error bars are standard deviations

deviation (RSD) of 28%, 39%, 8% and 3% for P, Ca, Fe and Al, respectively. Furthermore, results of repeated multi-elemental quantification in the reference soil material after every experimental soil sample analysis (error bars in Figure 1), show that the LA-ICP-MS measurements were consistent throughout the analysis.

### 3.2 | Spatially resolved multi-elemental distributions and concentrations in the forest soils

The average P concentration in the forest soils was spatially resolved by LA-ICP-MS imaging and compared with the pseudo-total ( $\text{HNO}_3$ -extractable) P concentrations in the same soils (Table 1).

The difference between the pseudo-total P and spatially resolved average P concentration ranged from 0.4 to 12.2  $\text{mmol kg}^{-1}$  and from 2.0 to 26.1  $\text{mmol kg}^{-1}$  at Tärnsjö and Tönnersjöheden, respectively. At Tärnsjö, both the spatially resolved and pseudo-total P concentrations were highest at 10–20 cm depth. However, pseudo-total P increased from 11.8  $\text{mmol kg}^{-1}$  at 40–50 cm depth to 17.2  $\text{mmol kg}^{-1}$  at 90–100 cm depth, whereas the spatially resolved P decreased from 15.3 to 5.0  $\text{mmol kg}^{-1}$ . At Tönnersjöheden, both the spatially resolved and pseudo-total P followed a similar abundance pattern, with P increasing with depth and reaching maximum concentrations at 20–50 cm depth before the concentration decreased.

Apart from the spatially resolved average-P reaching the highest concentration at 10–20 cm depth in Tärnsjö,

**TABLE 1** Pseudo total P (mmol kg<sup>-1</sup>) concentrations in bulk soils, multi-elemental concentrations (mmol kg<sup>-1</sup>) at spots with the highest P concentrations and average P concentrations (mmol kg<sup>-1</sup>) in soils as spatially resolved by semi-quantitative LA-ICP-MS imaging

Horizon/depth	Pseudo- Total P	LA-ICP-MS										P (hs/av)
		P	Na	Mg	Al	Si	K	Ca	Mn	Fe		
<i>Tärnsjö</i>												
Bs 2–10 cm		Highest P spot	1043.3	92.0	15.1	8973.4	1782.3	21.7	0	0.9	395.9	72
	15.0	Average	14.6 ± 2.7	272.7 ± 18.9	26.9 ± 5.4	1456.6 ± 64.7	2645.1 ± 76.7	268.6 ± 10.9	73.8 ± 3.7	1.3 ± 0.2	181.1 ± 29.0	
Bs 10–20 cm		Highest P spot	1107.9	185.4	302.9	7554.7	3981.1	222.8	174.7	15.7	2999.2	35
	20.9	Average	31.3 ± 4.3	497.3 ± 14.6	48.7 ± 10.0	1845.4 ± 56.5	2868.8 ± 65.6	76.2 ± 7.7	150.9 ± 9.4	2.5 ± 0.5	250.2 ± 33.8	
C 40–50 cm		Highest P spot	3434.2	315.1	4.2	897.2	1710.8	230.3	6022.6	2.7	26.8	225
	11.8	Average	15.3 ± 2.9	232.1 ± 10.9	123.9 ± 11.7	1306.2 ± 37.9	2198.3 ± 45.2	85.8 ± 9.4	151.4 ± 13.1	8.1 ± 0.8	410.5 ± 21.6	
C 90–100 cm		Highest P spot	2542.0	104.4	10,978.1	942.1	2732.8	59.1	6657.6	37.4	781.2	513
	17.2	Average	5.0 ± 1.0	100.4 ± 8.7	187.2 ± 134.5	624.3 ± 35.6	1281.0 ± 66.0	62.9 ± 5.7	195.5 ± 0.4	6.6 ± 0.5	296.4 ± 31.8	
<i>Tönnersjöheden</i>												
A 0–10 cm		Highest P spot	741.9	90.6	49.6	2401.3	740.1	191.4	0	837.6	13,616.7	43
	8.3	Average	17.3 ± 4.1	159.1 ± 15.9	117.2 ± 20.6	1580.1 ± 34.7	2174.3 ± 83.8	81.7 ± 13.1	100.6 ± 16.1	21.5 ± 3.3	736.9 ± 32.4	
Bs 10–20 cm		Highest P spot	214.6	164.2	171.0	9313.5	3089.1	136.2	73.7	16.2	2635.0	7
	14.2	Average	29.8 ± 0.7	172.3 ± 15.7	208.0 ± 15.7	2370.0 ± 32.6	2501.5 ± 83.2	112.3 ± 10.4	183.2 ± 14.5	19.5 ± 1.5	795.7 ± 12.7	
Bs 20–30 cm		Highest P spot	8326.4	86.4	14.1	193.5	298.0	0	16,998.1	17.9	65.7	191
	17.5	Average	43.6 ± 2.3	176.6 ± 23.8	150.4 ± 19.3	2940.9 ± 39.4	2972.4 ± 103.3	84.1 ± 12.7	136.4 ± 28.1	12.2 ± 2.5	949.0 ± 36.2	
Bs 30–40 cm		Highest P spot	366.2	1159.0	16.9	3234.6	5850.9	40.4	229.5	1.7	440.0	10
	18.0	Average	36.7 ± 0.6	167.5 ± 20.3	179.5 ± 20.1	2997.5 ± 27.2	2740.1 ± 92.5	118.3 ± 11.1	153.6 ± 29.3	8.9 ± 1.4	707.4 ± 28.2	
Bs 40–50 cm		Highest P spot	551.4	153.9	210.3	8926.9	3716.9	418.4	0	1249.4	2190.3	13
	18.0	Average	43.4 ± 2.0	174.7 ± 16.9	193.4 ± 26.7	2524.9 ± 94.3	2024.5 ± 120.6	90.8 ± 10.8	221.4 ± 4.7	8.9 ± 1.3	755.3 ± 35.1	
C 90–100 cm		Highest P spot	8716.7	29.9	16.6	88.1	166.9	18.1	11,713.5	14.8	14.7	603
	12.5	Average	14.5 ± 3.2	224.2 ± 24.4	87.7 ± 18.2	1266.7 ± 57.7	2411.2 ± 118.7	224.9 ± 34.7	150.5 ± 26.7	5.3 ± 1.4	265.3 ± 38.5	

Note: P (hs/av) is the magnitude of P concentrations at the highest P spot (hs) over average (av) P concentrations as estimated by LA-ICP-MS imaging.

spatially resolved average Na, Al, and Si concentrations were also highest at this depth, whereas Fe and Mn reached the maximum concentration at 40–50 cm depth. However, the spatially resolved average Ca and Mg concentrations in Tärnsjö had different abundance distribution patterns. They increased with depth and reached maximum concentrations at 90–100 cm depth. At Tönnersjöheden, spatially resolved P, Al, Si, and Fe all reached maximum concentrations in the B horizon at 20–30 cm depth. Ca and Mg were of a similar distribution pattern with the Bs horizons having higher concentrations than the 0–10 cm and 90–100 cm depths. The Mn concentration was highest at 0–10 cm depth and decreased with depth, whereas Na and K were lowest at 90–100 cm depth.

To gain insight into the chemical composition of the spots with the highest P concentration across the soil profiles, the concentration of P and other elements at these spots were revealed by LA-ICP-MS (Table 1). Although the concentrations of important elements such as titanium, fluorine, barium, strontium, sulfur, and carbon were not measured, the elements (Si, Al, Fe, Ca, Na, Mg, K, P, and Mn) that were quantified at these spots are among the twelve most abundant elements in the Earth's crust (Fleischer, 1953; Yaroshevsky, 2006). In the spot with the highest P concentration in Tärnsjö 2–10 and 10–20 cm depths, Al, followed by Si and Fe were the most abundant. Together with P, these elements accounted for 99% and 95% of the total elements measured in the spots at these two depths, respectively. Instead of Fe, Ca followed by Si and Al were the most abundant elements in the spot with the highest P concentration in Tärnsjö 40–50 cm, and Mg followed by Ca and Si were the most abundant elements at the spot with the highest P concentration in Tärnsjö 90–100 cm. The spots with the highest P concentration in the topsoils of Tönnersjöheden were also enriched in Fe. The concentration of Fe at these spots was 73% and 17% of the total elements measured at the spots in Tönnersjöheden 0–10 and 10–20 cm, respectively. At these depths, Fe, Al, Si, and P accounted for 94%–96% of all measured elements in the spots with the highest P concentration. A similar pattern was observed at Tönnersjöheden 30–40 and 40–50 cm. However, Ca was the most enriched element in the spots with the highest P concentration at Tönnersjöheden 20–30 cm and 90–100 cm, accounting for 65 and 56% of all the elements measured in the spots at these depths, respectively.

The concentrations of P at the spots with the highest P concentration within the soil microsites were compared to their spatially resolved average concentrations in the two soil profiles (Table 1). In Tärnsjö, P in these localised spots was between 35 and 513 times greater than the average soil P concentrations, with the highest values

(3434 and 2542 mmol P kg<sup>-1</sup>) occurring at 40–50 cm and 90–100 cm depths, respectively. At Tönnersjöheden, the P concentrations of the spots with the highest P concentration were between 7 and 600 times greater than the average soil P concentrations, with the highest value (8716 mmol P kg<sup>-1</sup>) occurring at 90–100 cm depth.

### 3.3 | Phosphorus speciation revealed by spatial multi-elemental co-localizations

Of the elements known to influence the chemical speciation of P in soils, the concentration of Al was the highest across the soil profiles (Table 1). A tricolour co-localization analysis of P (red), Al (blue), and other elements (green) was therefore used to depict the spatial distribution of P species in the soils. In the Tärnsjö Bs horizons (2–10 and 10–20 cm depths), P was mostly retained in the pore spaces and at the edges of soil grains (Figure 2).

In these horizons, P was mainly co-localised with Al, Si, and Fe (the white patches in Figure 2), and to a lesser extent with Mn, Mg, and K (the white patches in Figure S1). In the Tärnsjö C horizons (40–50 and 90–100 cm depths), P in the pore spaces and the edges of soil grains were mainly co-localised with Si and Al. However, in spots where the P concentrations were higher than those of the pore spaces and grain edges, P was found to be co-localised with Ca, Mg, Si, and Al, and existing as inclusions within Al and Si-bearing soil particles (point 1–9 at 40–50 cm and point 1–4 at 90–100 cm depths in Figure 2 and Figure S1). The soil area occupied by each of these P hot spots ranged from 25 to 40 μm<sup>2</sup>.

In the soils at Tönnersjöheden, P at the A and B horizons were also retained at the pore spaces and the edges of soil grains. In these horizons, P was co-localised predominantly with Al, Si, and Fe (Figure 3).

Although there was evidence of P co-localization with Mn and Mg at the 10–20 and 20–50 cm depths, respectively (Figure S1), P co-localizations with Al, Si, and Fe were the dominant P associations. P co-localization with Ca was sporadic in these horizons as only a few spots of P-Ca associations were noticeable (p1 and p2 at 20–30 cm and 40–50 cm). In the C horizon in Tönnersjöheden, P in the pore spaces and at the grain edges was also co-localised mainly with Al, Si, and to a lesser extent with Fe. However, in areas where P concentrations were higher than those at the pore-spaces and grain edges (p1 to p3), P was co-localised mostly with Ca in discrete soil grains. The sizes of these P-Ca grains at spots (p1), (p2), and (p3) were 72 × 50 μm, 100 × 50 μm, and 152 × 100 μm, respectively.

To deduce the type of Ca-P minerals and their potential geochemical transformations at the spots of P

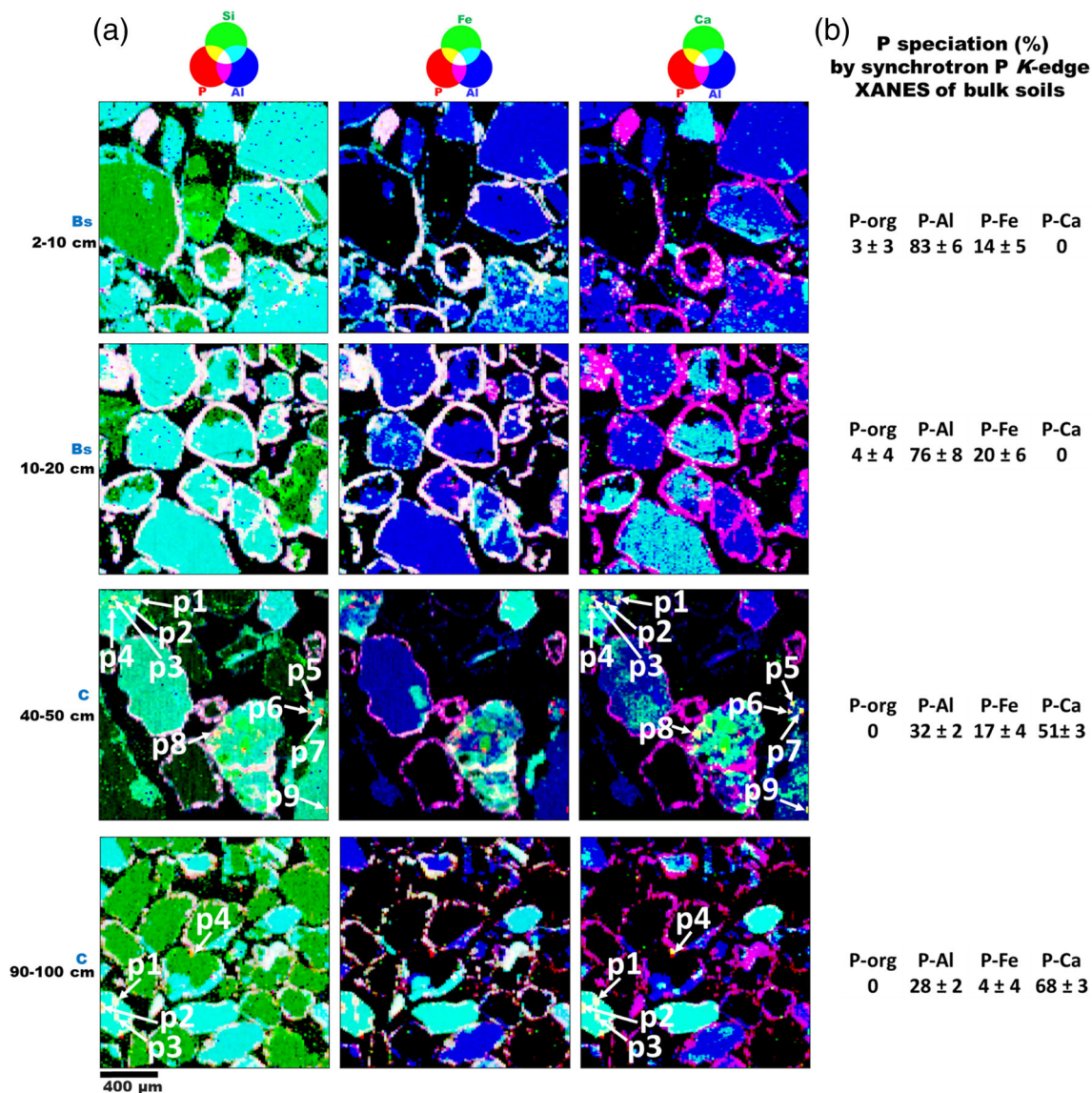


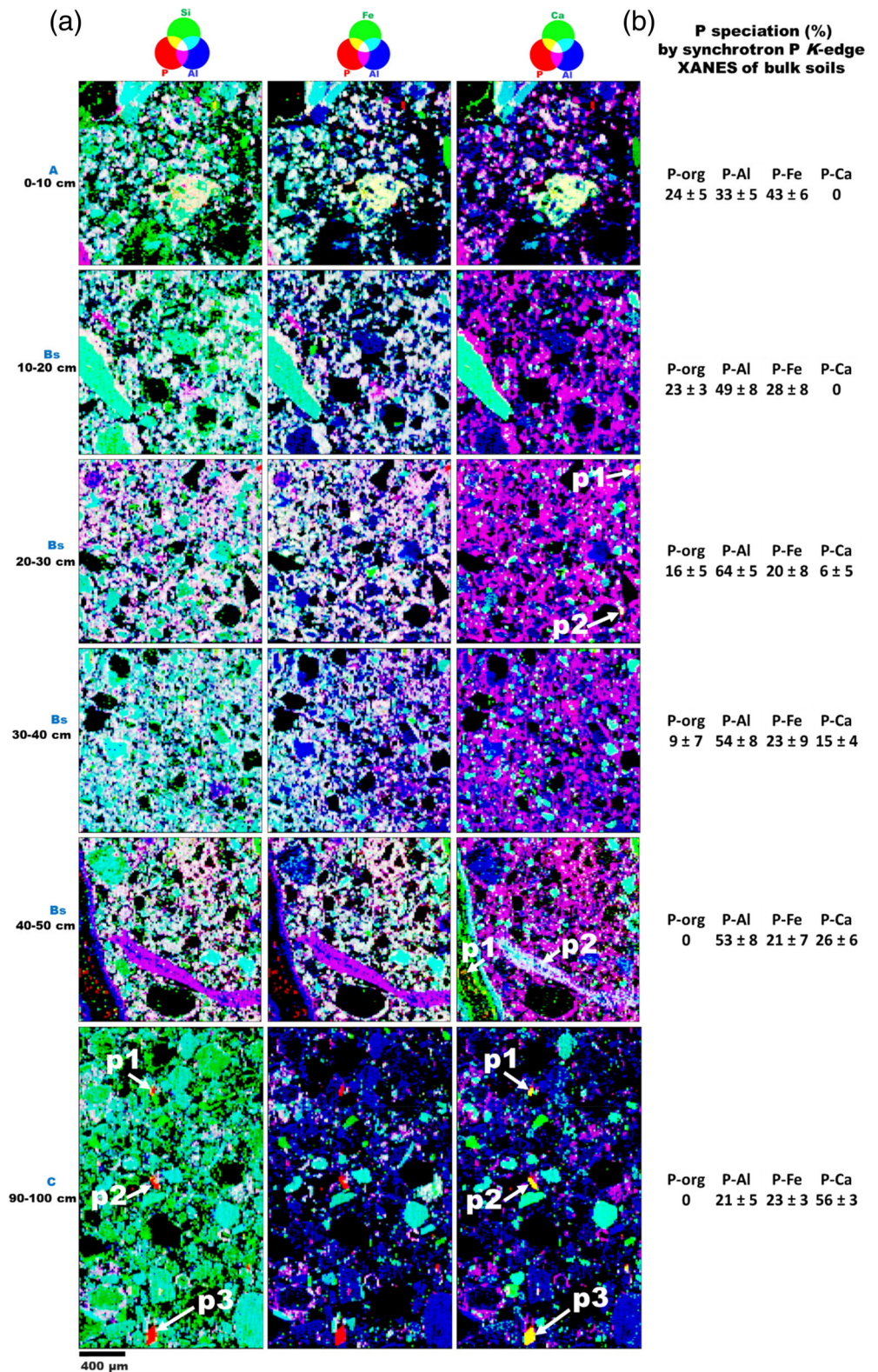
**FIGURE 2** Spatial co-localization of P with Si, Al, Fe, and Ca as revealed by LA-ICP-MS imaging and (b) P speciation by bulk soil P *K*-edge XANES in Tärnsjö soil profile. Figure shows points (p1–p9 at 40–50 cm and p1–p4 at 90–100 cm depths) of apatite inclusions. For the P *K*-edge XANES, P-org represent organic P, P-Al represents aluminium phosphate or P sorbed by allophane, P-Fe represents iron phosphate or P bound by ferrihydrite, and Ca-P represents apatite or calcium phosphate

inclusions and discrete grains, the concentrations of P and other elements were estimated from the same point, on and ( $\sim 10 \mu\text{m}$ ) around the highest P concentrated spot at several areas of P inclusions and discrete grains. Relative elemental abundance, as well as spot-wise Ca/P ratios, were then calculated (Table S2).

In the spots of P inclusions in Tärnsjö 40–50 cm depth, Si, followed by Ca and Al had the highest concentrations with a relative abundance that ranges between 20%–48%, 13%–45%, and 11%–22% respectively. These elements with P accounted for up to 86% of total elemental concentrations at these spots. The Ca/P ratio at these spots ranged from  $1.60 \pm 0.3$  to  $6.92 \pm 0.4$  with an

average of  $4.32 \pm 0.5$  across the spots (Table S2). However at 90–100 cm depth of the Tärnsjö soil, Mg followed by Ca and Si was the most concentrated, with a relative abundance that ranged between 29%–53%, 18%–32%, and 4%–34% respectively across the points of P inclusions. These elements with P accounted for 89% of all measured elements at these spots. The Ca/P ratio at these spots ranged from  $3.12 \pm 0.4$  to  $5.57 \pm 1.4$  with an average of  $4.73 \pm 0.8$  across the spots. Furthermore, Ca was the most abundant element of the discrete P grains in Tönnersjöheden 90–100 cm. While the relative abundance of Ca alone ranged between 64 and 71% in these grains, Ca with P accounted for 93% of all detected

**FIGURE 3** (a) Spatial colocalization of P with Si, Al, Fe, and Ca as revealed by LA-ICP-MS imaging and (b) P speciation by bulk soil P *K*-edge XANES in Tönnersjöheden soil profile. Figure shows points (p1-p3) of discrete apatite grains at the C-horizon. For the P *K*-edge XANES, P-org represent organic P, P-Al represents aluminium phosphate or P sorbed by allophane, P-Fe represents iron phosphate or P bound by ferrihydrite, and Ca-P represents apatite or calcium phosphate



elements at these grains. The average Ca/P ratio of these grains was  $2.88 \pm 0.3$ . However, the Ca/P ratio at the largest grain (p3) in Tönnersjöheden was  $2.14 \pm 0.60$  (Table S2). The relationships between the average concentrations of Ca and P at the spots of P-Ca inclusions

and micron-sized grain in the C horizons of the soils are presented in Figure 4.

This shows that the Ca concentration at these spots increased with increasing P concentrations by 2.8-fold (Figure 4).

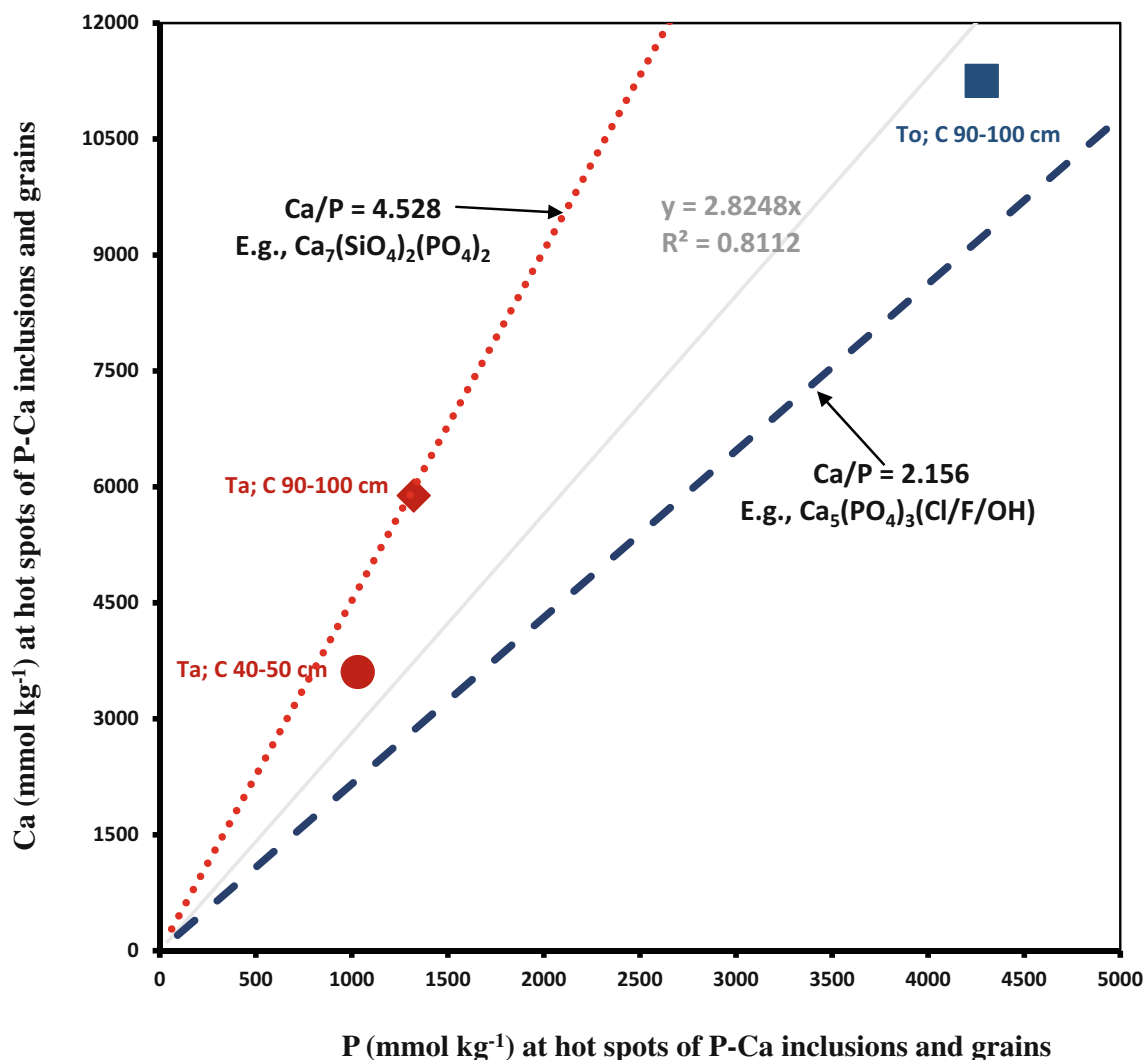


**FIGURE 4** Relationships between the average concentrations of Ca and P at the hot spots of P-Ca inclusions (red dots) and micron-sized grain (blue dot) in the C horizons at Tärnsjö (Ta) and Tönnersjöheden (To) respectively

## 4 | DISCUSSION

An observation that is common in most high-resolution microscale studies of P is that the P abundance is not evenly distributed in soils, as there are commonly unique spots of high P intensities even at the microscale (Adeiran et al., 2020; Hesterberg et al., 2017; Vogel et al., 2021; Werner, Mueller, et al., 2017; Yamaguchi et al., 2021). The significance of spatial heterogeneity in the concentrations of P at the microscale is, however, understudied. Here, we calibrated and validated the application of LA-ICP-MS for semi-quantitative multi-elemental analysis using ERM-CC141 certified reference soil material. We spatially resolved the concentrations of P and some elements known to influence its chemical speciation (e.g., Ca, Fe, and Al) in two Swedish forest soils. For these elements, the relative standard deviation (RSD) between the LA-ICP-MS measurements and the

certified concentrations ranged between 3% and 39%. In the work of Arroyo et al., where the use of LA-ICP-MS for soil analysis was evaluated and validated using soils that were grounded and well homogenised, an RSD of 8%–15% was reported (Arroyo et al., 2010). The precision of repeated multi-elemental measurements in our study ranged from 8%–15%. This range is similar to the 7%–15% reported by Arroyo et al. (2010).

Spatially resolved LA-ICP-MS imaging overestimated the pseudo-total P concentrations by a factor of ~1.02 across the depths in Tärnsjö, and by 2.22 and 1.16 at the 0–50 cm and 90–100 cm depths, respectively, at Tönnersjöheden. This difference in LA-ICP-MS measurements between the two soils is likely due to the differences in their texture and structure. For example, the Tärnsjö soil profile is (~97%) sandy, whereas the soils at the 0–50 cm depths of Tönnersjöheden are made up of ~86% sand, 10% silt, and 4% clay (Hansson et al., 2011). The soil

macropores are also more prominent in Tärnsjö than in Tönnersjöheden (Figures 2 and 3). Probably, P at Tönnersjöheden was incompletely extracted since P bound to constituents is not always completely dissolved by HNO<sub>3</sub> extraction. In turn, that P was likely detectable by LA-ICP-MS. This interpretation is supported by a recent survey of P interactions with soil particle fractions, which shows P to be more preserved in clay than in sand-sized fractions (Spohn, 2020). Moreover, considering that the elemental concentrations in the soil reference materials used for our LA-ICP-MS calibration were analysed on ground soil, our results of multi-elemental concentrations obtained by spatial imaging of un-ground soils are within an acceptable range for semi-quantitative analysis.

Our results show that the P concentrations at the high-P spots are 7 to 600 times greater than the average P concentrations. The estimation of average nutrient concentrations by bulk soil chemical extraction is the most widely used approach for assessing soil nutrient status. Therefore, these results are of significance to the interpretation of nutrient concentrations from bulk soil chemical extractions as most P concentrations obtained by traditional extraction methodologies may be from just a few micro-sized hot spots and discrete grains of high P intensities. Specifically, the results demonstrate that the soil system is a network of microsites with unique elemental concentrations. This agrees with the soil micro-chemical reactor concept, which states that “each soil microsite represents an independent but interconnected micro-reactor of unique chemical composition” (Hesterberg et al., 2011).

The distribution of P chemical species in the two soil profiles was previously studied by both spot-wise and bulk soils P K-edge XANES. This revealed inorganic P species as the predominant (~86% and 76% of the total P at Tärnsjö and Tönnersjöheden respectively) P forms in the soils (Adediran et al., 2020). Out of these inorganic P species, P K-edge XANES suggests apatite to be present mainly in the C horizons. P-Al was the most abundant P species in the B horizons of the soils, with most of the P-Al existing as phosphate bound to allophane (Adediran et al., 2020). These results are in agreement with the results of indirect P speciation analysis by multi-elemental imaging and co-localization presented in this study. This shows P to co-localise with both Al and Si mostly at the pore spaces and grain edges in the B horizons of the two soil profiles (Figures 2b and 3b). In our previous study, only one spot of apatite inclusion and one discrete grain of apatite were found in Tärnsjö and Tönnersjöheden respectively. This spot and grain were found only at the 90–100 cm depths of the two soils. However, the  $\mu$ XRF imaging in the previous study covered a soil area of 360 mm<sup>2</sup>, whereas a much larger soil area of

2560 mm<sup>2</sup> was analysed by LA-ICP-MS imaging in this study. The LA-ICP-MS imaging in this study shows that the Si and Al particles that are bearing the spots of P-Ca inclusions are about 1000  $\mu$ m apart (e.g., point 1 to point 5 at 40–50 cm depth). This study also shows that these P-bearing particles are present in the Tärnsjö C horizon from 40–50 cm to 90–100 cm depth. Similarly, at 90–100 cm depth in Tönnersjöheden, the discrete grains of P-Ca were about 700–1200  $\mu$ m apart.

Our previous study considered only qualitative imaging of P-Ca co-localization. In this study, we utilised spatially resolved LA-ICP-MS imaging to semi-quantitatively appraise the abundance of multiple elements at the spots of P inclusions and grains in the two soils. This shows that while Ca was the only enriched element in the discrete P grains in Tönnersjöheden, the spots of P inclusions in Tärnsjö are enriched not only in Ca but also in Si, Al, Mg and to a lesser extent, Fe. The Ca/P ratio in the two soils is consistent with those of apatite minerals, and these were probably inherited from the glaciofluvial parent material that formed the soils. This agrees with earlier research in which apatite was identified in glacial till with electron microscopy (Nezat et al., 2008).

Weathering in these soils is more intense in the A/E and B horizons and podzolisation processes have led to the enrichment of Fe and Al oxides/hydroxides and allophane/imogolite in the B horizons (Adediran et al., 2020; Tuyishime et al., 2022). The P concentration at some microsites in the A-B horizons was between 7 and 191 times larger than the average soil P concentration. However, in the C horizons where podzolization and weathering effects were less intense, there were spots, being 225 and 603 times more enriched in P than the average soil. Likely, due to the less intense weathering than in overlying horizons, part of the apatite still resides in the C horizons, either as inclusions within other mineral phases or even as discrete pure grains of apatite. Our results, therefore, affirm soil weathering and podzolization as the major factors governing the microscale heterogeneity in P speciation and concentration in these forest soils. By contrast, in the upper surface horizons, much of the rock-inherited apatite has been already weathered since the beginning of soil formation. The apatite weathering and podzolization processes were more intense in the A/E and B than in the C horizons. The speciation of the o-phosphate ions released from apatite was therefore strongly influenced by adsorption to the surfaces of allophane/imogolite and Fe hydrous oxides which are ubiquitous products of podzolization processes in the B horizons (Lundström et al., 2000). This interpretation is consistent with previous observations in soils of many temperate regions in which primary apatite was found to be absent or highly depleted in the upper 40 cm of the

soils (Eriksson et al., 2016; Walker & Syers, 1976; Werner, de la Haye, et al., 2017).

The Ca concentration at the P-Ca spots increased 2.8-fold with increasing P concentrations (Figure 4). As weathering intensifies, potential apatite dissolution in these soils is therefore of significance not only to P nutrition but also to the bioavailability and leaching of Ca (Akselsson et al., 2008; Yanai et al., 2005). It is expected that apatite inclusions will be more resistant to weathering than apatite grains because the release rate of included apatite depends to a large extent on the weathering rate of the host mineral (Syers et al., 1967). This is particularly important for apatite inclusion in minerals such as quartz, magnetite, and ilmenite as these are relatively resistant to weathering. For example, apatite enclosed in quartz was shown not to be affected by prolonged digestion with HCl and apatite inclusions in feldspar were found to persist even in a strongly acidic E horizon of a Dutch Podzol (Fry, 1913; Van Breemen et al., 2000). It is therefore likely that more P and Ca will be released from the apatite grains at Tönnersjöheden than from the P-Ca inclusions in Tärnsjö with progressing weathering.

## 5 | CONCLUSIONS

Micro-scale spatial distribution of P concentration and its co-localization with other elements has been successfully achieved by LA-ICP-MS analysis allowing us to for the first time characterise micron-sized areas of high P intensities. The P concentrations in these areas were 7 to 600 times greater than the bulk soil P concentrations. They exist as dispersed (~1000 µm apart) spots of P-Ca inclusions and discrete grains at 40–100 cm depth and 90–100 cm depth in Tärnsjö and Tönnersjöheden respectively.

Furthermore, P speciation analysis using co-localization with other elements agrees with previous speciation analysis by synchrotron XANES. In surface-near horizons, much of the P is bound to Al-Si and Fe phases, while in deeper horizons the P is mainly associated with Ca, Si, Al, and Mg (likely due to apatite inclusion within primary aluminosilicate mineral) and exclusively with Ca in discrete grains, likely consisting of pure apatite. Our results suggest that deeper soil horizons still hold substantial portions of apatite, while most apatite in the surface near horizons is already weathered. These findings reflect the state of pedogenesis of the studied soils.

## AUTHOR CONTRIBUTIONS

Conceptualization, Gbotemi A. Adediran and Jon-Petter Gustafsson; methodology, Gbotemi A. Adediran, Melanie Kielman-Schmitt, and Ellen Kooijman; data analysis, Gbotemi A. Adediran, Melanie Kielman-Schmitt, and

Ellen Kooijman; writing—original draft preparation, Gbotemi A. Adediran; writing—review and editing, Gbotemi A. Adediran, Jon-Petter Gustafsson, Melanie Kielman-Schmitt and Ellen Kooijman; project administration, Jon-Petter Gustafsson; funding acquisition, Gbotemi A. Adediran, and Jon-Petter Gustafsson.

## ACKNOWLEDGEMENTS

This work was funded by the Swedish Research Council Formas (grant number 2017-01139), and by the Geological Survey of Sweden (grant number 36-2044-2016). The LA-ICP-MS analysis was carried out at the Vegacenter laboratory at the Swedish Museum of Natural History. NordSIMS-Vegacenter is funded by the Swedish Research Council as a national research infrastructure (grant number 2021-00276). This is Vegacenter publication #058.

## CONFLICT OF INTEREST

The authors declare no conflict of interest.

## DATA AVAILABILITY STATEMENT

The data that support the findings of this study are presented in the supplementary material.

## ORCID

Gbotemi A. Adediran  <https://orcid.org/0000-0001-6657-3336>

Melanie Kielman-Schmitt  <https://orcid.org/0000-0002-5827-8043>

Ellen Kooijman  <https://orcid.org/0000-0003-2377-8272>

Jon-Petter Gustafsson  <https://orcid.org/0000-0001-8771-7941>

## REFERENCES

- Adediran, G. A., Tuyishime, J. M., Vantelon, D., Klysubun, W., & Gustafsson, J. P. (2020). Phosphorus in 2D: Spatially resolved P speciation in two Swedish forest soils as influenced by apatite weathering and podzolization. *Geoderma*, 376, 114550.
- Akselsson, C., Westling, O., Alveteg, M., Thelin, G., Fransson, A.-M., & Hellsten, S. (2008). The influence of N load and harvest intensity on the risk of P limitation in Swedish forest soils. *Science of the Total Environment*, 404, 284–289.
- Arroyo, L., Trejos, T., Gardinali, P. R., & Almirall, J. R. (2009). Optimization and validation of a laser ablation inductively coupled plasma mass spectrometry method for the routine analysis of soils and sediments. *Spectrochimica Acta Part B: Atomic Spectroscopy*, 64, 16–25.
- Arroyo, L., Trejos, T., Hosick, T., Machermer, S., Almirall, J. R., & Gardinali, P. R. (2010). Analysis of soils and sediments by laser ablation inductively coupled plasma mass spectrometry (LA-ICP-MS): An innovative tool for environmental forensics. *Environmental Forensics*, 11, 315–327.
- Beck, M., & Elsenbeer, H. (1999). Biogeochemical cycles of soil phosphorus in southern alpine spodosols. *Geoderma*, 91, 249–260.

- Blum, J. D., Klaue, A., Nezat, C. A., Driscoll, C. T., Johnson, C. E., Siccama, T. G., Eagar, C., Fahey, T. J., & Likens, G. E. (2002). Mycorrhizal weathering of apatite as an important calcium source in base-poor forest ecosystems. *Nature*, *417*, 729–731.
- Collins, T. J. (2007). ImageJ for microscopy. *BioTechniques*, *43*, S25–S30.
- Crews, T. E., Kitayama, K., Fownes, J. H., Riley, R. H., Herbert, D. A., Mueller-Dombois, D., & Vitousek, P. M. (1995). Changes in soil phosphorus fractions and ecosystem dynamics across a long chronosequence in Hawaii. *Ecology*, *76*, 1407–1424.
- Darcy, J. L., Schmidt, S. K., Knelman, J. E., Cleveland, C. C., Castle, S. C., & Nemerut, D. R. (2018). Phosphorus, not nitrogen, limits plants and microbial primary producers following glacial retreat. *Science Advances*, *4*, eaaq0942.
- Eriksson, A. K., Hillier, S., Hesterberg, D., Klysubun, W., Ulén, B., & Gustafsson, J. P. (2016). Evolution of phosphorus speciation with depth in an agricultural soil profile. *Geoderma*, *280*, 29–37.
- Filippelli, G. M. (2008). The global phosphorus cycle: Past, present, and future. *Elements*, *4*, 89–95.
- Fisher, D. J. (1973). Geochemistry of minerals containing phosphorus. In *The environmental phosphorus handbook*. Wiley.
- Fleischer, M. (1953). *Recent estimates of the abundances of the elements in the earth's crust* (Vol. 285). US Department of the Interior, Geological Survey.
- Fry, W. H. (1913). The condition of soil phosphoric acid insoluble in hydrochloric acid. *Industrial & Engineering Chemistry*, *5*, 664–665.
- Gustafsson, J. P., Akram, M., & Tiberg, C. (2015). Predicting sulphate adsorption/desorption in forest soils: Evaluation of an extended Freundlich equation. *Chemosphere*, *119*, 83–89.
- Gustafsson, J. P., Bhattacharya, P., & Karlton, E. (1999). Mineralogy of poorly crystalline aluminium phases in the B horizon of Podzols in southern Sweden. *Applied Geochemistry*, *14*, 707–718.
- Hansson, K., Olsson, B. A., Olsson, M., Johansson, U., & Kleja, D. B. (2011). Differences in soil properties in adjacent stands of scots pine, Norway spruce and silver birch in SW Sweden. *Forest Ecology and Management*, *262*, 522–530.
- Heindel, R. C., Lyons, W. B., Welch, S. A., Spickard, A. M., & Virginia, R. A. (2018). Biogeochemical weathering of soil apatite grains in the McMurdo dry valleys, Antarctica. *Geoderma*, *320*, 136–145.
- Hesterberg, D., Duff, M. C., Dixon, J. B., & Vepraskas, M. J. (2011). X-ray microspectroscopy and chemical reactions in soil microsites. *Journal of Environmental Quality*, *40*, 667–678.
- Hesterberg, D., McNulty, I., & Thieme, J. (2017). Speciation of soil phosphorus assessed by XANES spectroscopy at different spatial scales. *Journal of Environmental Quality*, *46*, 1190–1197.
- Högberg, P., Näsholm, T., Franklin, O., & Högberg, M. N. (2017). Tamm review: On the nature of the nitrogen limitation to plant growth in Fennoscandian boreal forests. *Forest Ecology and Management*, *403*, 161–185.
- IUSS Working Group WRB. (2014). World reference base for soil resources 2014. International soil classification system for naming soils and creating legends for soil maps. World Soil Resources Reports No. 106. FAO, Rome.
- Lanari, P., Vidal, O., De Andrade, V., Dubacq, B., Lewin, E., Grosch, E. G., & Schwartz, S. (2014). XMapTools: A MATLAB©-based program for electron microprobe X-ray image processing and geothermobarometry. *Computers & Geosciences*, *62*, 227–240.
- Larsen, S. (1967). Soil phosphorus. In *Advances in agronomy* (pp. 151–210). Elsevier.
- Lundström, U. S., van Breemen, N., & Bain, D. (2000). The podzolization process. A review. *Geoderma*, *94*, 91–107.
- Nezat, C. A., Blum, J. D., Yanai, R. D., & Hamburg, S. P. (2007). A sequential extraction to determine the distribution of apatite in granitoid soil mineral pools with application to weathering at the Hubbard brook experimental Forest, NH, USA. *Applied Geochemistry*, *22*, 2406–2421.
- Nezat, C. A., Blum, J. D., Yanai, R. D., & Park, B. B. (2008). Mineral sources of calcium and phosphorus in soils of the northeastern United States. *Soil Science Society of America Journal*, *72*, 1786–1794.
- Parfitt, R. (1989). Phosphate reactions with natural allophane, ferrihydrite and goethite. *Journal of Soil Science*, *40*, 359–369.
- Paton, C., Hellstrom, J., Paul, B., Woodhead, J., & Hergt, J. (2011). Iolite: Freeware for the visualisation and processing of mass spectrometric data. *Journal of Analytical Atomic Spectrometry*, *26*, 2508–2518.
- Porder, S., & Hillel, G. E. (2011). Linking chronosequences with the rest of the world: Predicting soil phosphorus content in denuding landscapes. *Biogeochemistry*, *102*, 153–166.
- Prietzl, J., Dümig, A., Wu, Y., Zhou, J., & Klysubun, W. (2013). Synchrotron-based P K-edge XANES spectroscopy reveals rapid changes of phosphorus speciation in the topsoil of two glacier foreland chronosequences. *Geochimica et Cosmochimica Acta*, *108*, 154–171.
- Santner, J., Larsen, M., Kreuzeder, A., & Glud, R. N. (2015). Two decades of chemical imaging of solutes in sediments and soils—a review. *Analytica Chimica Acta*, *878*, 9–42.
- Schlesinger, W. H., Bruijnzeel, L., Bush, M. B., Klein, E. M., Mace, K. A., Raikes, J. A., & Whittaker, R. (1998). The biogeochemistry of phosphorus after the first century of soil development on Rakata Island, Krakatau, Indonesia. *Biogeochemistry*, *40*, 37–55.
- Spohn, M. (2020). Phosphorus and carbon in soil particle size fractions: A synthesis. *Biogeochemistry*, *147*, 225–242.
- Stelly, M., & Pierre, W. (1943). Forms of inorganic phosphorus in the C horizons of some Iowa soils 1. *Soil Science Society of America Journal*, *7*, 139–147.
- Syers, J., Williams, J., Campbell, A., & Walker, T. (1967). The significance of apatite inclusions in soil phosphorus Studies<sup>1</sup>. *Soil Science Society of America Journal*, *31*, 752–756.
- Tuyishime, J. M., Adediran, G. A., Olsson, B. A., Spohn, M., Hillier, S., Klysubun, W., & Gustafsson, J. P. (2022). Phosphorus abundance and speciation in acid forest Podzols—effect of postglacial weathering. *Geoderma*, *406*, 115500.
- Van Breemen, N., Finlay, R., Lundström, U., Jongmans, A. G., Giesler, R., & Olsson, M. (2000). Mycorrhizal weathering: A true case of mineral plant nutrition? *Biogeochemistry*, *49*, 53–67.
- Vincent, A. G., Schleucher, J., Gröbner, G., Vestergren, J., Persson, P., Jansson, M., & Giesler, R. (2012). Changes in organic phosphorus composition in boreal forest humus soils: The role of iron and aluminium. *Biogeochemistry*, *108*, 485–499.
- Vogel, C., Helfenstein, J., Massey, M. S., Sekine, R., Kretzschmar, R., Beiping, L., Peter, T., Chadwick, O. A.,

- Tamburini, F., & Rivard, C. (2021). Microspectroscopy reveals dust-derived apatite grains in acidic, highly-weathered Hawaiian soils. *Geoderma*, 381, 114681.
- Walker, T., & Syers, J. K. (1976). The fate of phosphorus during pedogenesis. *Geoderma*, 15, 1–19.
- Werner, F., de la Haye, T. R., Spielvogel, S., & Prietzel, J. (2017). Small-scale spatial distribution of phosphorus fractions in soils from silicate parent material with different degree of podzolization. *Geoderma*, 302, 52–65.
- Werner, F., Mueller, C. W., Thieme, J., Gianoncelli, A., Rivard, C., Höschel, C., & Prietzel, J. (2017). Micro-scale heterogeneity of soil phosphorus depends on soil substrate and depth. *Scientific Reports*, 7, 3203.
- Westheimer, F. H. (1987). Why nature chose phosphates. *Science*, 235, 1173–1178.
- Williams, J., Mayer, T., & Nriagu, J. (1980). Extractability of phosphorus from phosphate minerals common in soils and sediments. *Soil Science Society of America Journal*, 44, 462–465.
- Yamaguchi, N., Ohkura, T., Hikono, A., Hashimoto, Y., Suda, A., Yamamoto, T., Ando, K., Kasuya, M., Northrup, P., & Wang, S.-L. (2021). Microscale heterogeneous distribution and speciation of phosphorus in soils amended with mineral fertilizer and cattle manure compost. *Minerals*, 11, 121.
- Yanai, R. D., Blum, J. D., Hamburg, S. P., Arthur, M. A., Nezat, C. A., & Siccama, T. G. (2005). New insights into calcium depletion in northeastern forests. *Journal of Forestry*, 103, 14–20.
- Yaroshevsky, A. (2006). Abundances of chemical elements in the Earth's crust. *Geochemistry International*, 44, 48–55.
- Zaeem, M., Nadeem, M., Pham, T. H., Ashiq, W., Ali, W., Gillani, S. S. M., Moise, E. R., Leier, H., Kavanagh, V., &

Galagedara, L. (2021). Development of a hyperspectral imaging technique using LA-ICP-MS to show the spatial distribution of elements in soil cores. *Geoderma*, 385, 114831.

Zetterberg, T., Olsson, B. A., Löfgren, S., von Brömssen, C., & Brandtberg, P.-O. (2013). The effect of harvest intensity on long-term calcium dynamics in soil and soil solution at three coniferous sites in Sweden. *Forest Ecology and Management*, 302, 280–294.

Zhou, J., Wu, Y., Prietzel, J., Bing, H., Yu, D., Sun, S., Luo, J., & Sun, H. (2013). Changes of soil phosphorus speciation along a 120-year soil chronosequence in the Hailuoguo glacier retreat area (Gongga Mountain, SW China). *Geoderma*, 195, 251–259.

## SUPPORTING INFORMATION

Additional supporting information can be found online in the Supporting Information section at the end of this article.

**How to cite this article:** Adediran, G. A., Kielman-Schmitt, M., Kooijman, E., & Gustafsson, J.-P. (2022). Significance of phosphorus inclusions and discrete micron-sized grains of apatite in postglacial forest soils. *European Journal of Soil Science*, 73(5), e13310. <https://doi.org/10.1111/ejss.13310>